Received: 30 July 2024 | Revised: 9 September 2024 | Accepted: 20 September 2024 | Published online: 25 September 2024

RESEARCH ARTICLE

Archives of Advanced Engineering Science
2025, Vol. 3(2) 83–92
DOI: 10.47852/bonviewAAES42023989

BON VIEW PUBLISHING

Numerical Investigation on Enhanced Thermal Performance of Rectangular Microchannels with Triangular Ribs

Md Nadimul Akram[1,*], Kazi Mohiuddin[2], Md Al Shahriar Akash[3], Felix Ibeh[4] and Md Shohel Kibria[5]

[1]*School of Energy and Environment, Southeast University, China*

[2]*College of Transport and Communications, Shanghai Maritime University, China*

[3]*School of Integrated Circuit, Southeast University, China*

[4]*College of Economics and Management, Shanghai Maritime University, China*

[5]*Technology Maritime & Built Environment, University of Highlands & Islands, United Kingdom*

Abstract: Effective thermal management becomes crucial with the rising heat produced by electronic devices. Microchannel convection shows excellent potential as a cooling solution. This study employs numerical computational techniques to examine rectangular microchannels' flow and heat transfer parameters on a semi-octagonal structure, specifically focusing on the Reynolds number (*Re*) ranging from 100 to 500. An extensive analysis evaluates the heat transfer design and hydraulic performance. Furthermore, the microchannel's diodic performance is assessed by comparing the Nusselt number (*Nu*) and the pressure drop in both the forward and backward directions. The study demonstrates the excellent performance of the microchannels within the microstructure under low *Re* conditions, emphasizing the significance of preserving the fundamental geometric characteristics while improving the fluid dynamics within the microchannel. The semi-octagonal structure microchannel design surpasses the conventional design in bidirectional heat transfer by improving spatial fluid mixing. With a *Re* of 300, the *Nu* of this microchannel surpasses that of the traditional rectangular design by a considerable margin. In addition, at this *Re*, the thermal diodicity (Di_t) and pressure drop diodicity (Di_p) showed significant improvements, with values of 1.16 and 1.45, respectively. Therefore, this study comprehensively compares the enhanced heat transfer of microchannel walls under constant heat flux, highlighting the advantages of semi-octagonal structural design in improving heat transfer and hydraulic performance. The results show that this innovative design has great potential to improve the efficiency of microchannel cooling and provides an important reference for the development of efficient thermal management systems.

Keywords: semi-octagonal structure, triangular ribs, fluid mixing, convectional heat transfer, diodic performance

1. Introduction

The single-phase microchannel heat sink is an incredibly effective cooling solution for many different applications, including air conditioning systems, battery cooling systems, and electrical equipment [1–3]. This is due to its high surface-to-volume ratio. Consequently, the traditional heat sink of single-phase microchannels cannot meet the stringent requirements for cooling relatively high-power electronic equipment. Several active and passive techniques can significantly improve convection heat transport in microchannels. Active strategies typically yield better results but require more external pumping power [4, 5]. Several studies have been conducted to confirm the continuum theory for incompressible fluid flows in microchannels, including three-dimensional heat transfer of solid and liquid phases in microchannel heat sinks [6, 7]. The microchannel width is significantly greater than the mean free path of the liquid phase, making traditional momentum and energy conservation calculations relevant. Passive strategies include introducing nanoparticles into the fluid, modifying microchannel surfaces, and designing boundary structures. For instance, heat transport capability can be significantly enhanced by adding nanoparticles with better thermal conductivity [8]. To evaluate the thermal-hydraulic performance of the microchannel with triangle cavities in the sidewalls, arranged rectangular ribs in the channel center core flow [9]. It was discovered that the flow disturbance, the thermal boundary layer interruption and redevelopment, and the chaotic mixing of hot and cool fluid greatly increased heat transfer. Microchannel heat sink design has improved heat transfer by generating disturbances with passive microstructures like dimple surfaces, groove structures, ribs, and cavities. Cylindrical micro fins significantly reduce thermal resistances. Simulated a three-dimensional grooved microchannel heat sink to study

***Corresponding author:** Md Nadimul Akram, School of Energy and Environment, Southeast University, China. Emails: 223227060@seu.edu.cn; nadim.akram684679@gmail.com

geometrical parameter effects on forced convection heat transfer characteristics [10]. Numerous studies have been conducted to enhance the thermal-hydraulic performance of microchannels with cavities and ribs, as seen in the literature review above. However, determining the optimal channel combination is crucial for optimizing microchannel performance. Further research is needed to identify novel designs that can improve thermal performance while minimizing pressure drops.

Extended research has been conducted to increase fluid mixing by exploring several microchannel shapes such as the fins, small cylinders, baffles, and winglets, examining the effects of cavities in microchannels on the fluid flow and convection [11–14]. A thorough analysis of the microchannel's overall performance with a periodic tapered segment was carried out. Their findings showed that the Nusselt number (*Nu*) was raised by 12.5–27.2% compared to the conventional rectangular (CR) microchannel [15]. A numerical simulation analyzed heat transfer in microchannel heat sinks with varied header forms (trapezoid, triangular, and rectangular) and inlet/outlet locations (Z, C, and I type). This simulation included four distinct channel cross-sections: standard, offset fan-shaped, sawtooth, and triangular [16–18]. In contrast to earlier research that improved convective heat transfer using different geometry [19], the current study suggests a unique semi-octagonal structure microchannel that was motivated by a microfluidic rectifier [20, 21]. Increasing the wall area of a flowing fluid reduces system irreversibility due to temperature differences. It increases pressure drop to sustain flow [22, 23], which was investigated with triangular ribs or microchannel side walls with a semi-octagonal form. It was projected that Model 1 would perform better when combined with a trapezoidal rib up to *Re* 300 and a triangular rib for greater *Re*. The placement of ribs in microchannel heat sinks enhances their thermal performance and increases flow resistance due to the intensified flow disturbance. This makes it unsuitable for boosting heat transfer when dealing with higher *Re*.

On the other hand, cavities can improve heat transfer by increasing fluid mixing and interrupting and redeveloping the thermal barrier layer while maintaining a suitable pressure drop. To take advantage of the improved thermal performance of ribs and the reduced flow resistance, specific novel designs of microchannels have been suggested that incorporate ribs and a semi-octagonal structure. These designs effectively boost heat transfer while minimizing the pressure drop. A novel microchannel design that includes both cavities and ribs on the sidewalls has also been introduced [24], and experimentation has shown that the influence of various rib types on the overall performance is noticeable.

This microfluidic rectifier's single-phase diodicity has been measured up to 1.50. Nonetheless, the influence of this microchannel with a semi-octagonal structure on convective heat transfer efficiency remains. Two models of semi-octagonal structure microchannel designs are being studied to enhance heat transmission by disrupting thermal barrier layers and increasing fluid mixing. Numerical research evaluates how a semi-octagonal structure affects convection and fluid mixing in a single channel. We studied the diode properties of the microchannels of the semi-octagonal structure and analyzed the pressure increase and thermal properties in the forward and backward directions, respectively. This study aims to highlight the superiority of our design by comparing the numerical results of our microchannel design with the results of CR microchannels and other related studies.

2. Problem Statement

For cooling electronics, single-phase heat sinks with many microchannels are frequently used. To effectively disperse heat from electrical components, this design frequently utilizes a schematic shown in Figure 1. In this work, flow and heat transfer within individual microchannels of a heat sink are studied by

Figure 1
(a) Top and side view of microchannel with boundary conditions. (b) 3-D view of three different microchannel configurations

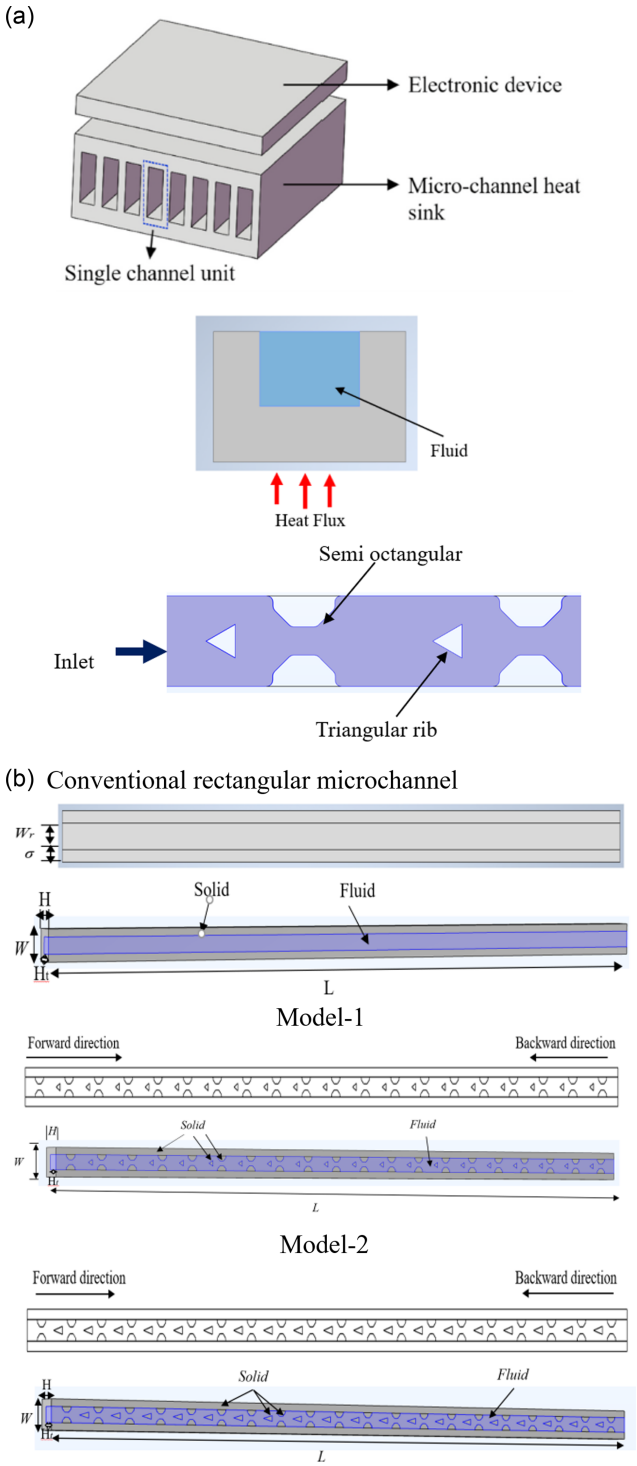

numerical simulations. Three different microchannel layouts have been devised, encompassing a CR microchannel and two models of semi-octagonal structure microchannel, which are Model 1 and Model 2. The heat sink dimensions are height = 0.7 mm, width = 1.28 mm, and length = 30 mm. Rectangular microchannel height is $H_t = 0.4$ mm, and width is $W_r = 0.6$ mm. 0.6 mm is the average width of the semi-octagonal structure microchannel, and the wall thickness is $\sigma_t = 0.28$ mm. The flow rate and heat transfer properties in the microchannel with the semi-octagonal structure and internal triangular ribs in the water-based fluid and copper-based solid because copper has high thermal conductivity, excellent corrosion, and ease of manufacture used under a constant heat flux have been explored in this study. The dimensional specifics for various microchannel configurations are present in Table 1.

Table 1
Different microchannel configurations and dimensions

Parameters	Values
Length (L)	30000 μm
Width (W)	1280 μm
Height (H)	700 μm
Length (Lt)	188 μm
Single channel height (H_t)	400 μm
Wall thickness (σ_t)	280 μm
Rectangular channel width (W_r)	600 μm
F. Channel width (W_f)	600 μm
B. Channel width (W_b)	600 μm
Model 1 triangular ribs (height + width)	244 μm + 244 μm
Model 2 triangular ribs (height + width)	244 μm + 422 μm

3. Numerical Technique

3.1. Governing equations

A solid-fluid conjugate mathematical model is used to model thermal-hydrodynamic performance in all three dimensions. The assumptions for this study include the following:

1) The fluid Newtonian is steady, laminar, and incompressible.
2) The physical parameters of the microchannel are consistent.
3) The environment's loss of heat may be overlooked.
4) No phase change occurs in the heat transfer process of the fluid.

Based on the assumptions mentioned above, throughout this investigation, the following governing equations have been used:

$$\Delta . u_i = 0 \tag{1}$$

$$u_i \rho . \Delta u_i = -\Delta p + \mu \Delta^2 u_i \tag{2}$$

$$c_p \rho \left(u_i . \Delta T_f\right) = k_f \Delta^2 T_f + \phi \tag{3}$$

The energy equation for conduction is derived by:

$$k_s \Delta^2 T_s = 0 \tag{4}$$

where specific heat, velocity, and fluid density are c_p, ρ, and u accordingly. Copper thermal conductivity, water, the temperature of the fluid, and temperature of solid are k_s, k_f, T_f, and T_s accordingly. ϕ is the expression of the ratio at which mechanical energy is transformed into heat energy as a result of viscous friction. Additionally, the fluid thermophysical characteristics (density, internal energy, specific heat capacity, and thermal conductivity) may be computed and depend on temperature. These COMSOL-built formulas provide the temperature dependency of the fluid characteristics. Furthermore, the fluid thermophysical properties (ρ, u, cp, and kf) can be determined based on temperature [25, 26].

$$\begin{aligned}
\rho(T_f) &= 838.466135 + 1.40050603\ T_f - 0.0030112376\ T_f^2 \\
&\quad + 3.718222313 * 10^{-7} T_f^4 \\
\mu(T_f) &= 1.3799566804 - 0.021224019151\ T_f \\
&\quad + 1.3604562827 * 10^{-10} T_f^2\ - 4.6454090319 * 10^{-7} T_f^3 \\
&\quad + 8.9042735735 * 10^{-10} T_f^4\ - 9.0790692686 * 10^{-13} T_f^5 \\
&\quad + 3.8547331488 * 10^{-16} T_f^6 \\
c_p(T_f) &= 12010.1417 - 80.4072879 T_f\ + 0.309866854 T_f^2 \\
&\quad - 5.38186884 * 10^{-4} T_f^3 + 3.62536437 * 10^{-7} T_f^4 \\
k_f(T_f) &= -0869083936 + 0.00894880345 T_f + 1.5866345 \\
&\quad * 10^{-5} T_f^2 + 7.9543259 * 10^{-9} T_f^3
\end{aligned} \tag{5}$$

3.2. Boundary conditions

Model 1 for rectangular microchannels establishes specific boundary conditions mirrored in the simulation of both conventional microchannels and Model 2 rectangular microchannels. A consistent heat load of 150000 W/m^2 is delivered to the rear surface, and all side walls are adiabatic, as shown in Figure 1(a). It is assumed that the heat sink mechanism of heat transmission is conjugate heat transfer. The sidewalls are set as no-slip velocity boundaries ($u_{non-slip} = 0$). Solid interface $T_s = T_f$ and $k_s \frac{\partial T}{\partial n}|_r = k_f \frac{\partial T_f}{\partial n}|_r$. T is the solid wall's interface with liquid. The specified *Re* from 100 to 500 determined the flow velocity at the inlet. While 293.23 K is the inlet temperature, it remained constant. Zero pressure was enforced at the outlet, and the no-slip condition was applied to the microchannel walls. The upper limit was considered as adiabatic (Figure 2).

3.3. Grid and validation

The proper mesh size and structure significantly impact the accuracy of numerical simulations. Figure 3 shows some of the structured meshes used in various microchannel designs. The mesh surface was extruded using the standard method and contained small features. A mesh independence check was performed to ensure the accuracy of the numerical results. Table 2 lists the information on the mesh studies. The governing equations were solved using Comsol Multiphysics 6.0, a commercial software that uses the finite element method. The number of elements corresponding to different mesh sizes was analyzed specifically 3.1 million, 5.4 million, and 10 million. In this case, 5.4 million grid nodes are used. Table 2 compares the fluid outlet temperature, pressure drop, and average solid temperature of a semi-octagonal structured microchannel with the results of a fine mesh example for *Re* of 100 and 300. The results show that the outlet fluid temperature complies with the law of energy

Figure 2
Boundary conditions: (a) Microchannel cross-section area. (b) Top view of the computational domain

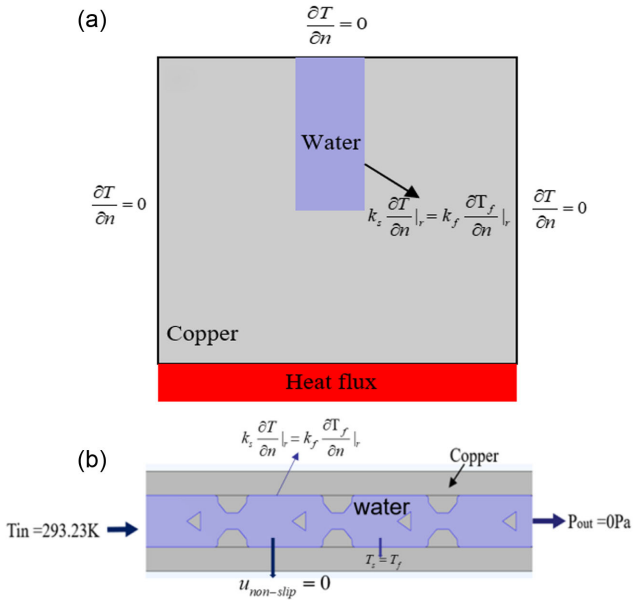

Figure 3
Microchannel close-up view of mesh

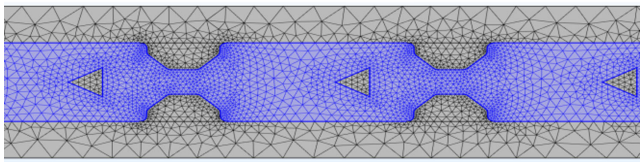

Table 2
Grid information

No.	Grid number	Re	Solid temperature average (K)	Outlet fluid temperature (K)	Pressure drop (Pa)
1	3111040	100	368.93	400.43	513.12
		300	300.33	311.30	12529.06
2	5474819	100	366.16	401.20	516.1
		300	302.33	311.56	12829.21
3	10859901	100	369.70	400.32	514.23
		300	301.88	310.66	12940.10

conservation in all three cases. One validation study was conducted on a CR microchannel without cavities, while the other studies were conducted on a semi-octagonal microchannel with triangular ribs on the sidewalls. All boundary conditions in the previous and current numerical studies are consistent, except for those at the inlet and outlet. This study shows that numerical results obtained with the finite difference method by Qu and Mudawar [27]. Copper and DI (deionized) water are considered. A steady wall heat flux of 150 W/cm^2 is applied to the bottom wall conditions, while the other walls remain adiabatic. The output thermal resistance $R_{t,out}$ is displayed for Reynolds values between 100 and 500 and defined $R_{t,out}$ as:

$$R_{t,out} = \frac{T_{w,out} - T_{in}}{q_w''} \quad (6)$$

where T_{in} and $T_{w,out}$ represent the inlet fluid and top wall temperature and heat flux is q_w''. The numerical results closely correspond to the reported values. At low *Re*, there is an insignificant deviation. The reason for this exception is the dissipation of thermal energy. According to Figure 4, the highest relative error between the numerical model used in this study and previous studies is approximately 11.4%. This suggests that the simulations conducted in this study are accurate and reliable.

Figure 4
Comparisons of the current model with earlier numerical analyses

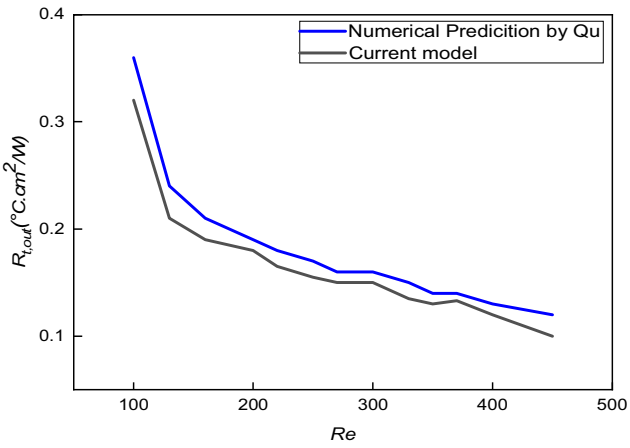

The area of heating and inlet indicates the microchannel's cross-sectional and bottom areas. As shown in Figure 5, the temperature difference relative inaccuracy is less than 4.5%, verifying the correctness of the current simulation.

Figure 5
Temperature differences between theoretical and simulation results

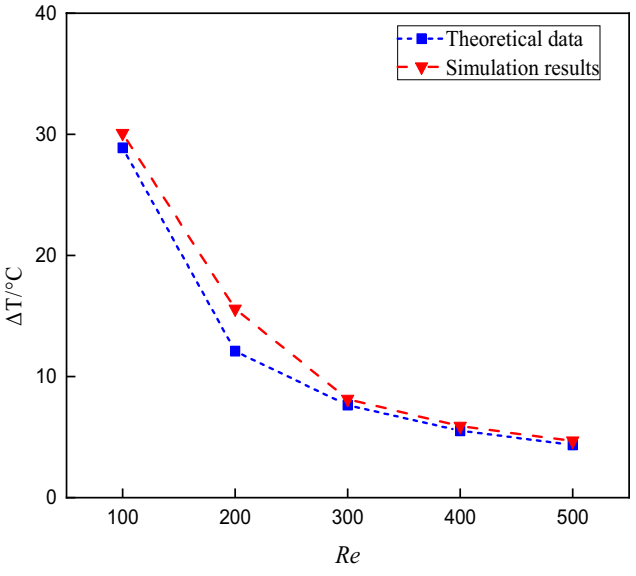

3.4. Data reduction

There is an accumulation of numerical data regarding pressure drop, temperature, *Re*, flow velocity, heat transfer coefficient (HTC), *Nu*, and other related parameters. The *Re* is calculated by:

$$\mathrm{Re} = \frac{\rho u_m D_h}{\mu} \tag{7}$$

where hydraulic diameter and dynamic viscosity are D_h, u_m, and μ. The hydraulic diameter is identified by:

$$D_h = \frac{2HW}{(H+W)} \tag{8}$$

The hydraulic diameter is estimated in this work using the average width of a semi-octagonal structure microchannel. So, it is calculated by:

$$W = \frac{W_1 + W_2}{2} \tag{9}$$

Here, minimum and maximum width can be found as W_1 and W_2 in this semi-octagonal structure microchannel. Pressure drop can be found as:

$$\Delta P = P_{in} - P_{out} \tag{10}$$

Di_p (Pressure drop diodicity) is pressure drop ratio in opposite directions

$$Di_p = \frac{\Delta P_b}{\Delta P_f} \tag{11}$$

where forward direction and backward directions represent ΔP_f, ΔP_b and pressure drop. Moreover, the efficiency of heat transfer can be defined by averaged HTC, which may be indicated as:

$$h = \frac{q''_w A_h}{A_c\left(T_{w.ave} - T_{f.ave}\right)} \tag{12}$$

Average *Nu* is obtained by:

$$Nu_{ave} = \frac{hD_h}{k_f} \tag{13}$$

Here, A_c and A_h are an area of convective heat transfer (accordingly, the surface area of the fluid contact and the inner fluid/solid wall) and the area of the heating surface (heat sink of the bottom surface). $T_{f.ave}$ and represents the average temperature of fluid and surface average temperature. The ratio of *Nu* in the forward and backward directions is known as thermal diodicity Di_t.

$$Di_t = \frac{Nu_B}{Nu_F} \tag{14}$$

The forward and backward Nussle numbers represent as Nu_F and Nu_B, respectively. To evaluate ribbed microchannel hydrodynamic performance and thermal comprehensively, performance evaluation criteria (PEC) can be used in this study [28, 29].

$$PEC = \frac{Nu/Nu_0}{(f^-/f^-_0)^{1/3}} \tag{15}$$

The equation mentioned above has the symbol 0 to denote the results of CR microchannels. Average friction (f^-) can be expressed by:

$$f^- = \frac{\Delta P D_h}{2\rho L {u_m}^2} \tag{16}$$

Here, microchannel length is L, and average intel fluid velocity is u_m.

4. Result and Discussion

4.1. Properties of fluid flow

A numerical study of triangular ribs was conducted to determine the effect of rib shape on fluid flow characteristics. The plane closest to the wall was selected as an ideal place to analyze the fluid and heat transfer characteristics of flow boiling in ribbed channels. Figures 6 and 7 show the velocity distribution of flow streamlines in the plane (z = 0.4 mm) between the x and y directions when the *Re* is 100 to 500 in different microchannel configurations. The results show that the flow structure of triangular rib microchannels is significantly different from that of CR microchannels. The semi-octagonal rib

Figure 6
Three different microchannel designs' flow field variation at Reynolds number 100

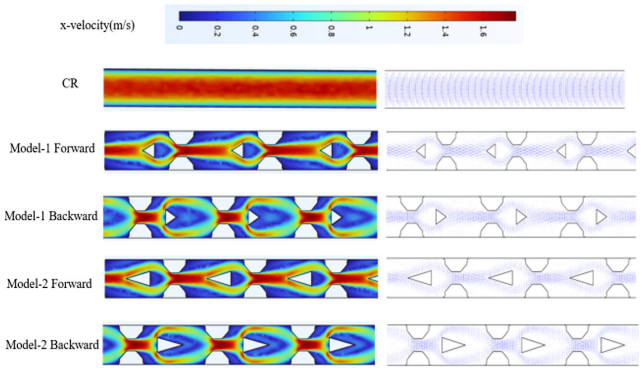

Figure 7
Three different microchannel design flow field variations at Reynolds number 500

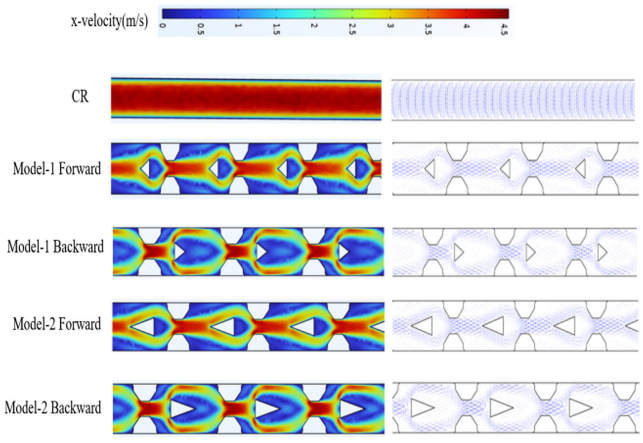

shape disturbs the flow characteristics and significantly destroys the fluid boundary layer. By introducing semi-octagonal structural units into the flow field, the vortex in the Model 2 microchannel extends to a wider area. When *Re* increases to 500, the fluid mixing and vortex in the semi-octagonal microchannel are enhanced, especially in the downstream area. When *Re* is 500, the vortex area becomes more prevalent and significant. The semi-octagonal periodic interruption of the microchannel continuously splits, elongates, and destroys the fluid boundary layer. In addition, the semi-octagonal microchannel's downstream velocity gradient is smaller than the upstream velocity gradient, further promoting interlayer mixing. Figure 7 shows the variation of this velocity gradient in detail. Through the periodic perturbations of these structures, the fluid boundary layer is frequently destroyed and reconstructed, thereby improving the fluid mixing efficiency and heat transfer performance. This flow and heat transfer characteristic shows that the semi-octagonal microchannel has significant advantages in enhancing mixing and heat transfer.

4.2. Comprehensive thermal efficiency

Figure 8 shows the temperature distribution in the x-y plane for different microchannels when the *Re* is 500. The results show that the triangular rib microchannel can effectively reduce the wall temperature (*Tw*) and fluid temperature, especially at the rib height. Due to the effect of convective heat transfer, the fluid temperature gradually increases along the flow direction. As shown in Figure 8, in all microchannels, the area between the two octagonal structures near the leading edge shows a higher temperature because the velocity in this area is reduced. Compared with the Model 1 and Model 2 microchannels, the *CR* microchannel has the lowest fluid temperature at the center of the microchannel, showing comparable thermal performance. However, the fluid temperature distribution of the semi-octagonal structure microchannel is more uniform. This indicates that the fluid mixing and periodic disturbance in the semi-octagonal structure microchannel significantly improve the heat transfer rate. Moreover, the reverse flow of the semi-octagonal microchannel also shows superior thermal performance, as shown in Figures 7 and 8. The semi-octagonal structure promotes fluid mixing by periodically destroying and rebuilding the fluid boundary layer, thereby improving heat transfer efficiency. This design has significant advantages in terms of enhanced thermal performance, indicating that at high *Re*, the half-octagonal microchannels can be more effective in thermal management.

4.3. Diodic performance

This study evaluates the diode performance of a specific design, focusing on the pressure drop fluctuation in two rectangular microchannel configurations. Figure 9 shows the difference in the pressure drop diode performance in the Model 1 and Model 2 setups. When the *Re* is low, the pressure drop is close to 1.24, but when the *Re* increases to 500, the pressure drop rises to about 1.45. Thermal diode performance is another important component of diode performance, and it is calculated using Equation (14). In this work, the diodic performance of a specific design is evaluated, concentrating on the fluctuation of pressure drop in two configurations of rectangular microchannels. Figure 10 represents the differences in pressure drop diodicity for both setups Model 1 and Model 2. The pressure drop in both the forward and backward flow directions is higher in Model 2 compared to Model 1. First, the average *Nu* for reverse flow is obtained, as shown in Figure 11. The *Re* significantly affects *Nu* because as *Re* increases, convection is enhanced, resulting in improved fluid flow, which affects *Nu* and the thermal diode performance of the system. In the heat transfer performance comparison, Model 1 outperforms Model 2 for rectangular microchannels on a semi-octagonal structure. At a *Re* of 300, the *Nu* of the microchannels of Model 1 in the forward and backward directions are 52.44 and 60.67, respectively. The *Nu* values of the rectangular microchannels on the semi-octagonal structure of model 2 are 62.39 and 65.86, respectively. This indicates that the microchannels of Model 2 have better heat transfer capabilities than Model 1 and exhibit higher *Nu* values in the above case. Figure 12 shows the relationship between *Dit* and *Re*. The results show that with the increase of *Re*, the thermal performance is significantly improved, with *Dit* as high as 1.16. This enhancement is mainly attributed to the semi-octagonal structure promoting spatial fluid mixing, thereby considerably enhancing the reverse thermal conductivity.

Figure 8
Temperature of different microchannels when *Re* 500

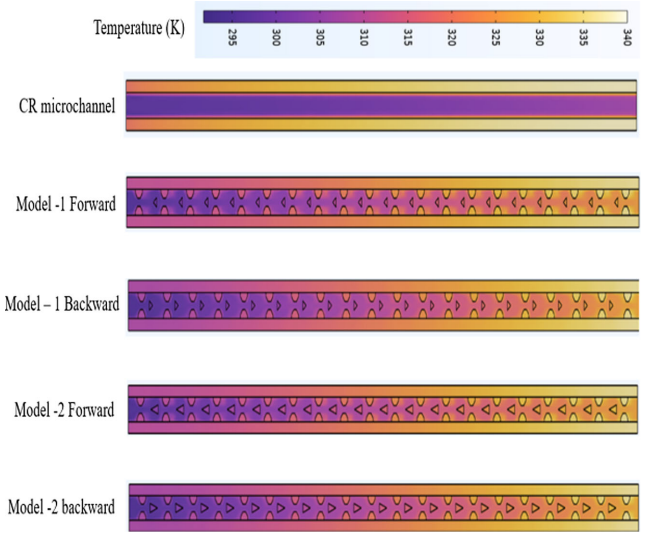

Figure 9
Pressure diodicity *Dip* versus *Re*

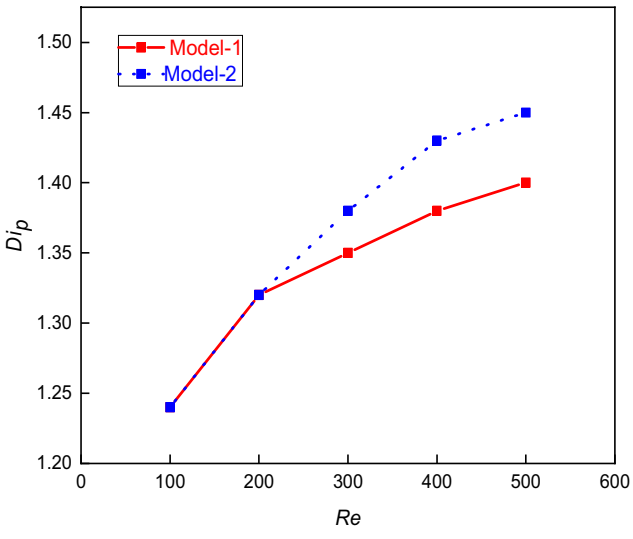

Figure 10
Pressure drop versus *Re*

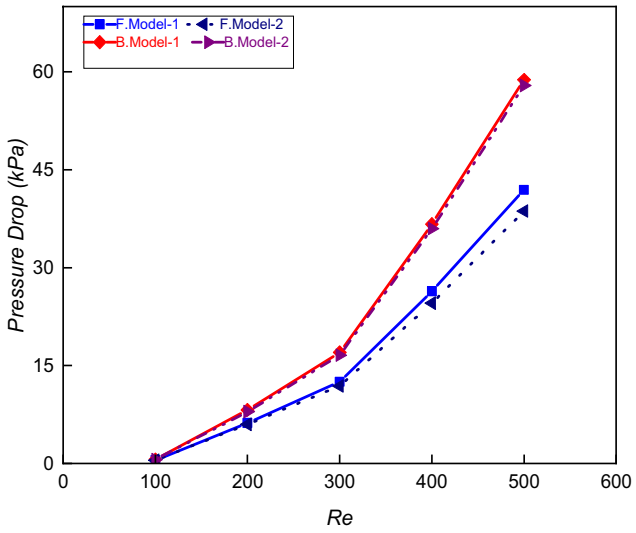

Figure 11
The difference between *Nu* and *Re*

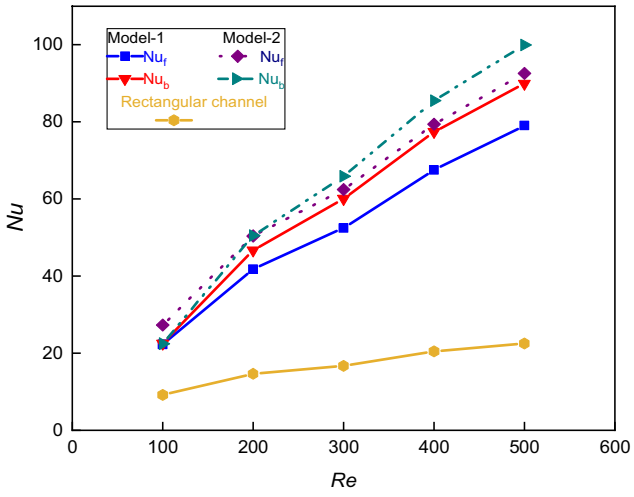

4.4. Effect of ribs on fluid flow

One potential remedy is to create a heat sink system with heat dissipation ribs and enhanced heat transfer performance. To this end, the fluid flow characteristics of a heat sink system with a semi-octagonal geometry and the effect of the aspect ratio of the triangular ribs on its performance have been investigated. In all analyses, other parameters remain constant. The length of the major axis of the triangular ribs in Model 1 remains constant at 0.2 mm. The height of model 2 is 0.224 mm, while the height of the other two regions is 0.442 mm. Figures 6 and 7 show the three-dimensional pressure and velocity distributions in the plane parallel to the (x, y) plane, respectively, revealing the complex heat transfer dynamics in the triangular rib heat sink system with different semi-octagonal structures. The pressure field shows regions of various intensities, reflecting the flow behavior and the resistance distribution, while the velocity field highlights the

Figure 12
Thermal diodicity *Dit* versus *Re*

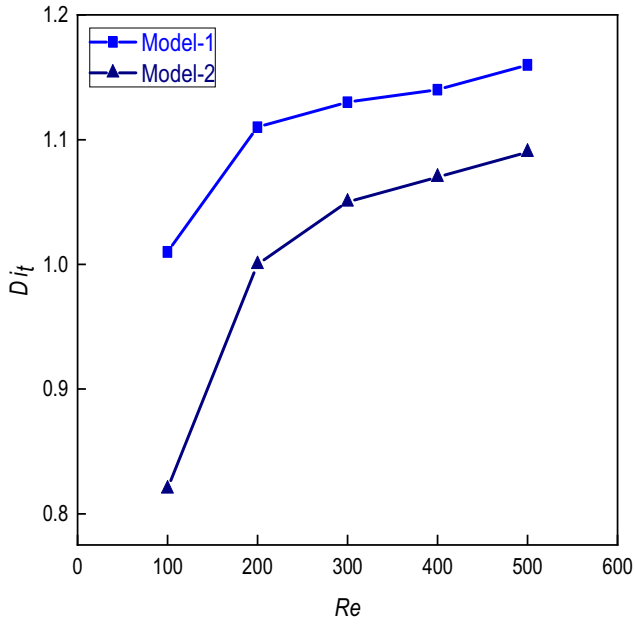

momentum direction of the fluid flow. Specifically, the pressure distribution map reveals the changes in resistance encountered by the fluid when passing through different structural regions, which directly affect the overall pressure drop of the system. The velocity distribution map shows the direction and velocity magnitude of the fluid flow, revealing the existence of vortices, recirculation regions, and high- and low-velocity regions. These distribution plots help understand how the triangular ribs and half-octagonal structures affect the flow path of the fluid and the heat transfer efficiency. By analyzing these plots, the heat sink design can be optimized to enhance the heat transfer performance and reduce the system's pressure drop, thereby improving the overall thermal management efficiency.

4.5. Convection heat transfer improvement

The results of this study are analyzed in detail and compared with previous studies that have investigated the mechanism of enhanced thermal/hydraulic performance within semi-octagonal microchannels. Figure 13 shows the *Nu* (*Nu*/*Nu*0) versus the *Re* for Model 1 and Model 2, where Nu0 represents the *Nu* in a CR channel. In Model 1, the average improvement across all data points is approximately 204.90%. For Model 2, the average improvement is approximately 263.13%. Figure 13 shows the relative *Nu* at different *Re* calculated using this formula *Nu*/*Nu*0, where *Nu* is Model 1 and Model 2 *Nu* in both case forward and backward directions and *Nu*0 represents a CR microchannel. Based on early results Figure 13 made. The relative *Nu* at different *Re* provides insight into how the effectiveness of heat transfer enhancement varies with the flow regime. If the relative *Nu* is greater than 1, it shows that the enhancement is effective even in laminar flow. So our result is greater than 1, which means enhanced flow and heat transfer. The results show that the *Nu* for the two semi-octagonal microchannel configurations investigated in this study are much larger than those reported earlier. This suggests that the semi-octagonal microchannels' thermal and hydraulic performance is superior to the previously tested designs. Without a continuous array of enhancement units, the fluid mixing in the

Figure 13
Relative Nusselt number at different Reynolds numbers

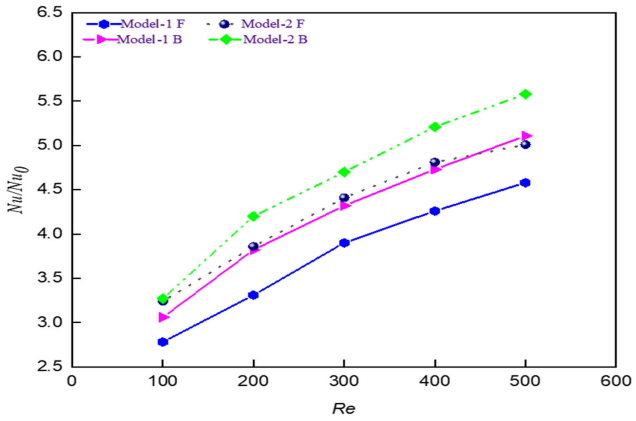

Figure 14
Variation of *PEC* versus *Re*

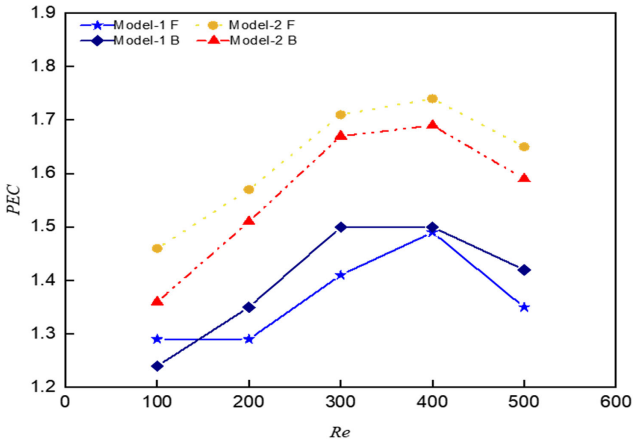

center is insufficient. However, the repeated semi-octagonal microchannels can effectively disrupt the boundary layer and promote three-dimensional fluid mixing, significantly enhancing convective heat transfer. The periodic semi-octagonal microchannels induce alternating vortices at different spatial locations through diverging-converging effects. This configuration ultimately improves the overall efficiency of heat exchange and fluid flow operations. Transverse and longitudinal vortices further enhance the three-dimensional fluid mixing and more effectively disrupt the boundary layer.

Figure 14 depicts the variation of the *PEC* with *Re* in Model 1 and Model 2 microchannels. Notably, the *PEC* value decreases significantly when the *Re* exceeds especially when it is less than 500. Model 2 microchannels perform better in helping the fluid flow forward especially at high *Re*. Overall, the results demonstrate the significant impact of channel type on fluid dynamics and highlight the advantages of Model 2 microchannels in specific operating scenarios.

Through these analyses, this study reveals the potential of semi-octagonal structured microchannels in enhancing heat transfer and hydraulic performance, especially for applications in complex fluid dynamics operations. These findings provide valuable guidance for optimizing heat dissipation systems and other engineering applications that require efficient thermal management.

5. Conclusions

This work thoroughly investigates the cooling performance of a semi-octagonal microchannel with triangular ribs placed near the semi-octagonal structure, emphasizing conjugate heat transfer processes. The thermal and hydraulic performance of the three configurations is rigorously examined through numerical studies. The configurations investigated include a CR channel and two semi-octagonal microchannels with triangular ribs. The comprehensive analysis focuses on the thermal and pressure drop characteristics, elucidating the inherent bidirectional nature of these parameters. We demonstrate the effectiveness of the semi-octagonal arrangement in improving convective heat transfer within microchannels. In particular, at a *Re* of 300, the heat transfer performance is significantly improved compared to the CR microchannel. This enhancement can be attributed to the enhanced spatial fluid mixing achieved by the unusual geometry of the semi-octagonal structure. The performance parameters of the thermal diode (*Dit*) and the pressure drop diode (*Dip*) are 1.16 and 1.45, respectively, at a *Re* of 300 for the semi-octagonal microchannel. These results highlight the greater directional control over thermal and pressure aspects within microchannels, demonstrating the practical relevance of our approach in thermal management applications. This innovative design significantly improved the microchannel system's cooling efficiency, demonstrating its potential for efficient thermal management.

Ethical Statement

This study does not contain any studies with human or animal subjects performed by any of the authors.

Conflicts of Interest

The authors declare that they have no conflicts of interest to this work.

Data Availability Statement

Data available on request from the corresponding author upon reasonable request.

Author Contribution Statement

Md Nadimul Akram: Conceptualization, Software, Validation, Formal analysis, Investigation, Writing – original draft. **Kazi Mohiuddin:** Methodology, Writing – review & editing, Visualization. **Md Al Shahriar Akash:** Resources, Data curation. **Felix Ibeh:** Validation, Formal analysis. **Md Shohel Kibria:** Supervision, Project administration.

References

[1] Tu, J., Qi, C., Li, K., & Tang, Z. (2022). Numerical analysis of flow and heat characteristic around micro-ribbed tube in heat exchanger system. *Powder Technology*, *395*, 562–583.

[2] Li, F., Ma, Q., Xin, G., Zhang, J., & Wang, X. (2020). Heat transfer and flow characteristics of microchannels with solid and porous ribs. *Applied Thermal Engineering*, *178*, 115639.

[3] Sikdar, P., Datta, A., Biswas, N., & Sanyal, D. (2020). Identifying improved microchannel configuration with triangular cavities and different rib structures through evaluation of thermal performance and entropy generation

number. *Physics of Fluids*, *32*(3), 033601. https://doi.org/10.1063/1.5137842

[4] Zhu, Q., Chang, K., Chen, J., Zhang, X., Xia, H., Zhang, H., . . . , & Jin, Y. (2020). Characteristics of heat transfer and fluid flow in microchannel heat sinks with rectangular grooves and different shaped ribs. *Alexandria Engineering Journal*, *59*(6), 4593–4609.

[5] Feng, Z., Zhou, C., Guo, F., Zhang, J., Zhang, Q., & Li, Z. (2023). The effects of staggered triangular ribs induced vortex flow on hydrothermal behavior and entropy generation in microchannel heat sink. *International Journal of Thermal Sciences*, *191*, 108331.

[6] Wang, G., Chen, T., Tian, M., & Ding, G. (2020). Fluid and heat transfer characteristics of microchannel heat sink with truncated rib on sidewall. *International Journal of Heat and Mass Transfer*, *148*, 119142.

[7] Paramanandam, K., Venkatachalapathy, S., & Srinivasan, B. (2022). Heat transfer enhancement in microchannels using ribs and secondary flows. *International Journal of Numerical Methods for Heat & Fluid Flow*, *32*(7), 2299–2319.

[8] Li, B., Cui, Y., Li, G., & Jiang, H. (2024). Numerical analysis on thermal-hydraulic performance of optimized microchannel heat sink with slant ribs and quatrefoil rib-elliptical groove complex structures. *Applied Thermal Engineering*, *240*, 122165.

[9] Zhu, Q., Su, R., Xia, H., Zeng, J., & Chen, J. (2022). Numerical simulation study of thermal and hydraulic characteristics of laminar flow in microchannel heat sink with water droplet cavities and different rib columns. *International Journal of Thermal Sciences*, *172*, 107319.

[10] Zhu, Q., Xia, H., Chen, J., Zhang, X., Chang, K., Zhang, H., . . . , & Jin, Y. (2021). Fluid flow and heat transfer characteristics of microchannel heat sinks with different groove shapes. *International Journal of Thermal Sciences*, *161*, 106721.

[11] Akcay, M., Ates-Kalkan, P. S., Ustundag, U. V., Unal, I., Cansız, D., Alturfan, E. E., & Alturfan, A. A. (2022). Determination of bisphenol A and phthalate levels in wastewater samples. *Experimed*, *12*(3), 134–138.

[12] Zhuang, D., Yang, Y., Ding, G., Du, X., & Hu, Z. (2020). Optimization of microchannel heat sink with rhombus fractal-like units for electronic chip cooling. *International Journal of Refrigeration*, *116*, 108–118.

[13] Hong, F. J., Cheng, P., Ge, H., & Joo, G. T. (2007). Conjugate heat transfer in fractal-shaped microchannel network heat sink for integrated microelectronic cooling application. *International Journal of Heat and Mass Transfer*, *50*(25–26), 4986–4998.

[14] Yang, F., Alwazzan, M., Li, W., & Li, C. (2014). Single- and two-phase thermal transport in microchannels with embedded staggered herringbone mixers. *Journal of Microelectromechanical Systems*, *23*(6), 1346–1358.

[15] Wang, C., Zhu, J., Li, H., Dai, D., Lv, H., & Lv, Q. (2024). Enhanced heat transfer study of microchannel heat sink with periodically arranged triangular cavities and arc-shaped ribs. *Heat Transfer*, *53*(5), 2438–2459.

[16] Lv, Q., Yan, T., Feng, Y., Huang, H., & Qin, J. (2024). Experimental and numerical study of flow boiling heat transfer characteristics in rectangular groove-wall microchannels. *International Journal of Heat and Mass Transfer*, *220*, 124999.

[17] Wang, S. L., Chen, L. Y., Zhang, B. X., Yang, Y. R., & Wang, X. D. (2020). A new design of double-layered microchannel heat sinks with wavy microchannels and porous-ribs. *Journal of Thermal Analysis and Calorimetry*, *141*, 547–558.

[18] Lu, K., Wang, C., Wang, C., Fan, X., Qi, F., & He, H. (2023). Topological structures for microchannel heat sink applications – A review. *Manufacturing Review*, *10*, 1–27.

[19] Porwal, P. R., Thompson, S. M., Walters, D. K., & Jamal, T. (2018). Heat transfer and fluid flow characteristics in multistaged Tesla valves. *Numerical Heat Transfer, Part A: Applications*, *73*(6), 347–365.

[20] Groisman, A., & Quake, S. R. (2004). A microfluidic rectifier: Anisotropic flow resistance at low Reynolds numbers. *Physical Review Letters*, *92*(9), 094501.

[21] Zeng, L., Deng, D., Zhong, N., & Zheng, G. (2021). Thermal and flow performance in microchannel heat sink with open-ring pin fins. *International Journal of Mechanical Sciences*, *200*, 106445.

[22] Zhai, Y. L., Xia, G. D., Liu, X. F., & Li, Y. F. (2015). Exergy analysis and performance evaluation of flow and heat transfer in different micro heat sinks with complex structure. *International Journal of Heat and Mass Transfer*, *84*, 293–303.

[23] Ayatollahi, S. M., Ahmadpour, A., & Hajmohammadi, M. R. (2022). Performance evaluation and optimization of flattened microchannel heat sinks for the electronic cooling application. *Journal of Thermal Analysis and Calorimetry*, *147*(4), 3267–3281.

[24] Zhai, Y. L., Xia, G. D., Liu, X. F., & Li, Y. F. (2014). Heat transfer in the microchannels with fan-shaped reentrant cavities and different ribs based on field synergy principle and entropy generation analysis. *International Journal of Heat and Mass Transfer*, *68*, 224–233.

[25] Al-Asadi, M. T., Alkasmoul, F. S., & Wilson, M. C. T. (2018). Benefits of spanwise gaps in cylindrical vortex generators for conjugate heat transfer enhancement in micro-channels. *Applied Thermal Engineering*, *130*, 571–586.

[26] Al-Asadi, M. T., Alkasmoul, F. S., & Wilson, M. C. T. (2016). Heat transfer enhancement in a micro-channel cooling system using cylindrical vortex generators. *International Communications in Heat and Mass Transfer*, *74*, 40–47.

[27] Qu, W., & Mudawar, I. (2002). Analysis of three-dimensional heat transfer in micro-channel heat sinks. *International Journal of Heat and Mass Transfer*, *45*(19), 3973–3985.

[28] Raihan, M. F., Al-Asadi, M. T., & Thompson, H. M. (2021). Management of conjugate heat transfer using various arrangements of cylindrical vortex generators in micro-channels. *Applied Thermal Engineering*, *182*, 116097.

[29] Webb, R. L. (1981). Performance evaluation criteria for use of enhanced heat transfer surfaces in heat exchanger design. *International Journal of Heat and Mass Transfer*, *24*(4), 715–726.

How to Cite: Akram, M. N., Mohiuddin, K., Akash, M. A. S., Ibeh, F., & Kibria, M. S. (2025). Numerical Investigation on Enhanced Thermal Performance of Rectangular Microchannels with Triangular Ribs. *Archives of Advanced Engineering Science*, *3*(2), 83–92. https://doi.org/10.47852/bonviewAAES42023989

Nomenclature

A_h: Surface of heating area, m^2
A_{in}: Inlet, m^2
A_c: Convection heat transfer area, m^2
D_h: Hydraulic diameter, m
Cp: Capacity of specific heat, J/(kg·K)
Di: Diodicity
Di_p: Pressure diodicit
Di_t: Thermal diodicity
f: Friction average
h: Coefficient of heat transfer, W/(m^2·K)
k_s: *Solid's* thermal conductivity, W/(m·K)
k_f: Fluid's thermal conductivity, W/(m·K)
L: Heat sink length, m
L_t: Single microchannel length, m
Nu_F: Forward direction of Nusselt number
Nu_B: Backward direction of Nusselt number
Nu_0: Nusselt number of the rectangular microchannel
P_{out}: Pressure outlet, Pa
q'': Heat flux, W/m^2
P_{in}: Pressure inlet, Pa
ΔP: Pressure drop, Pa
T: Temperature, K
$T_{b,ave}$: The average temperature of the solid surface
$T_{w,out}$: Temperature at the top wall of the heat sink, K
u: Velocity of the fluid in the x direction, m/s
u_m: Average velocity of the inlet fluid
W: Width of the heat sink's cross-section, m
W_r: Width of rectangular microchannel, m
W_b: Backward microchannel width, m
W_f: *Width of the* forward direction of microchannel,m

Greek symbols

ρ: Density, kg/m^3
Φ: function of viscous dissipation
μ: Dynamic viscosity, Pa·s
σ: Wall thickness, m

Appendix

0: Rectangular microchannel
out: Outlet
B: Backward
f: Fluid
ave: Average
s: Solid
F: Forward
in: Inlet